Supporting information

Conductivity Mechanism of Lithium Argyrodite Solid-State Electrolytes

1. Multivariate Regression Analysis of Experimental Data

Please see separate Excel Spreadsheet submitted along with the Manuscript and Supporting Information files (Table S1).

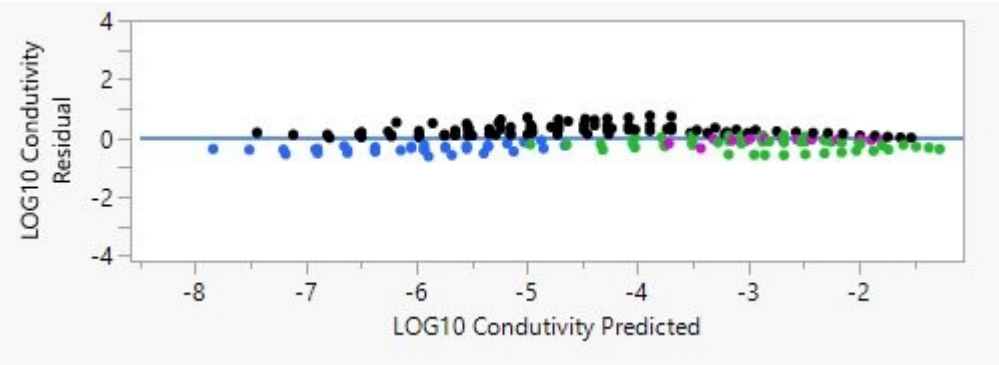

Figure S1. Residuals graph for Multivariate Log-Log linear regression model of Li_6PS_5X argyrodite conductivity as function of α_{4d} and $1/T$.

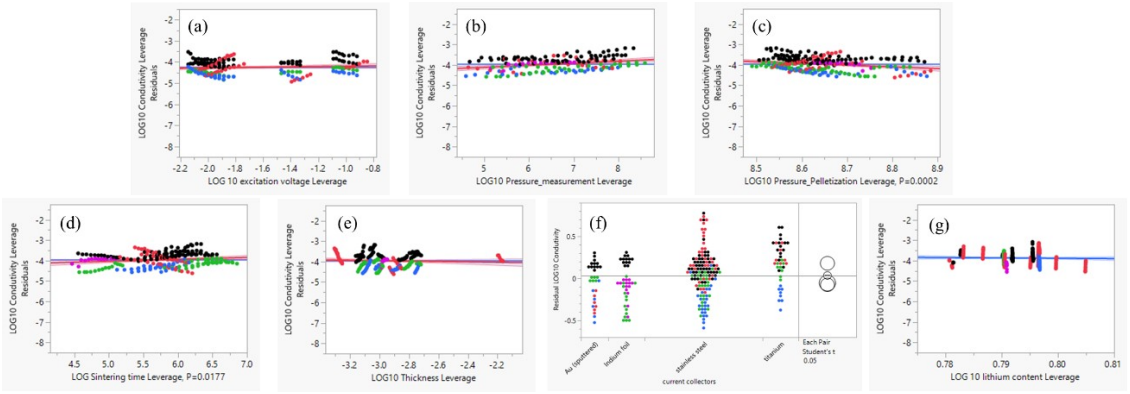

Figure S2. Partial conductivity Log-Log leverage as function of tested variables without a statistically significant effect on the conductivity of Li6PS5X conductivity. (a) Partial conductivity leverage as function of excitation voltage. (b) Partial conductivity leverage as function of experimental pressure. (c) Partial conductivity leverage as function of palletisation pressure. (d) Partial conductivity leverage as function of sintering time. (e) Partial conductivity leverage as function of pellet thickness. (f) Multi-variate t-test of the effect of different current collectors on the conductivity of argyrodite. (g) Partial conductivity leverage as function of lithium content.

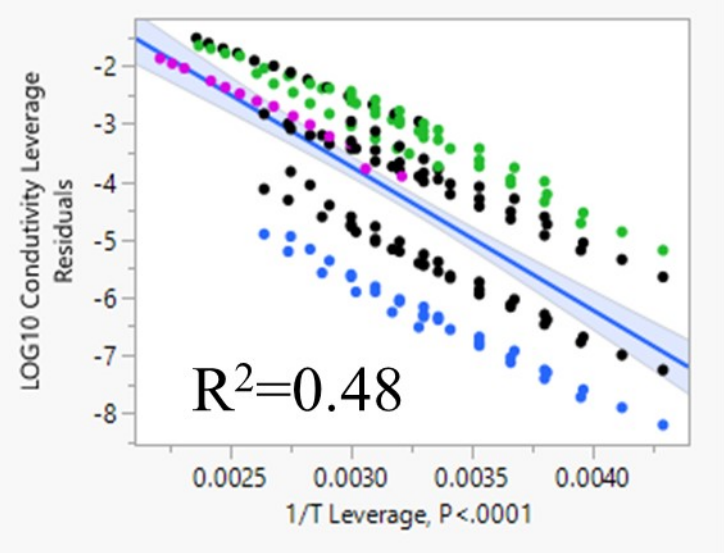

Figure S3. Regression model of Li_6PS_5X argyrodite conductivity as function of $1/T$ alone. Samples with higher α_{4d} exhibit higher conductivity values for the same temperature.

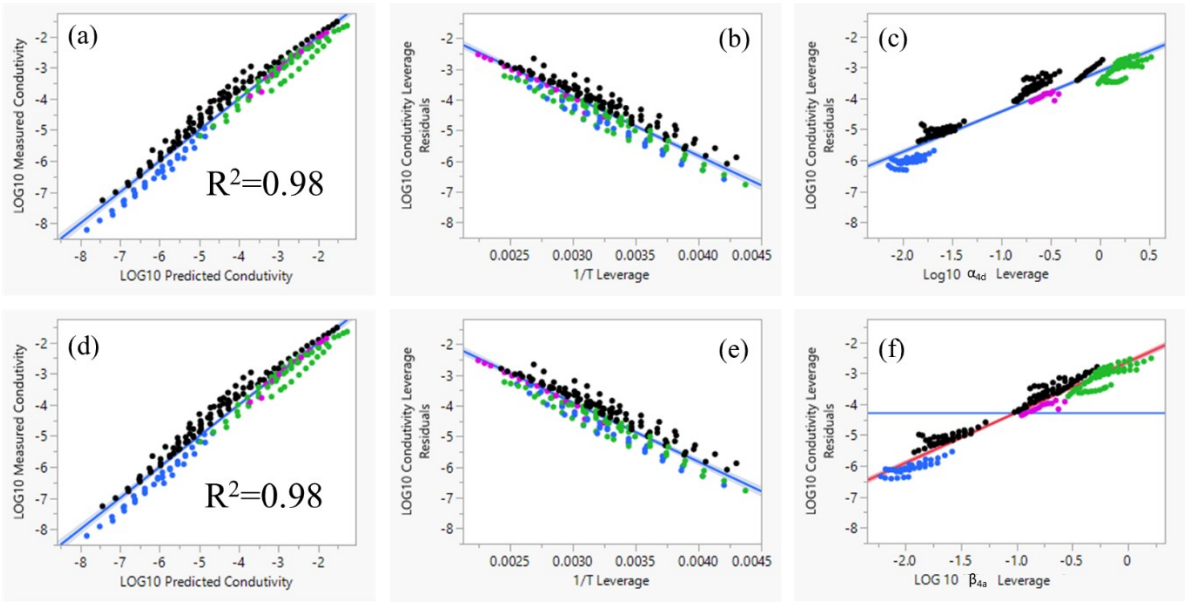

Figure S4. Comparison of multivariate Log-Log linear regression model of Li_6PS_5X argyrodite conductivity as function of α_{4d} and $1/T$ or β_{4a} and $1/T$. (a) Measured conductivity vs multivariate predicted conductivity. (b) Partial conductivity leverage as function of 1/T. (c) Partial conductivity leverage as function of α_{4d}. (d) Measured conductivity vs multivariate predicted conductivity. (e) Partial conductivity leverage as function of 1/T. (f) Partial conductivity leverage as function of β_{4a}.

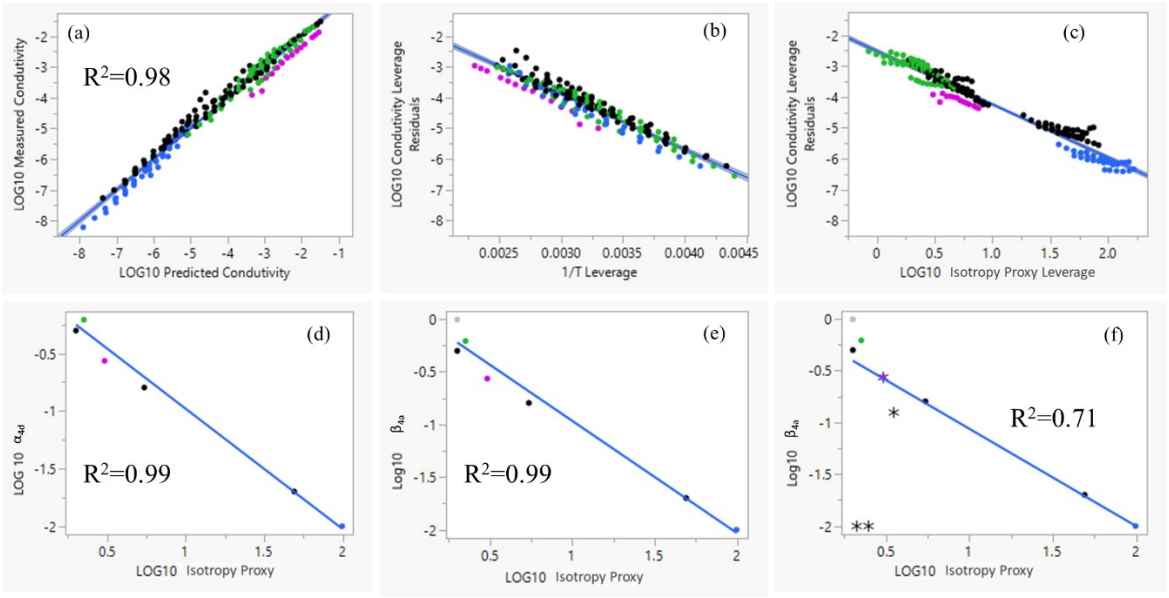

Figure S5. Multivariate Log-Log linear regression model of Li_6PS_5X argyrodite conductivity as function of isotropy proxy and $1/T$. (a) Measured conductivity vs multivariate predicted conductivity. (b) Partial conductivity leverage as function of 1/T. (c) Partial conductivity leverage as function of $\left|\frac{1-\beta_{4a}}{\alpha_{4d}}+\frac{1-\alpha_{4d}}{\beta_{4a}}\right|$. (d) Correlation between α_{4d} and $\left|\frac{1-\beta_{4a}}{\alpha_{4d}}+\frac{1-\alpha_{4d}}{\beta_{4a}}\right|$ for Li_6PS_5X. (e) Correlation between β_{4a} and $\left|\frac{1-\beta_{4a}}{\alpha_{4d}}+\frac{1-\alpha_{4d}}{\beta_{4a}}\right|$ for $Li_6PS_5X + Li_7PS_6$. (f) Correlation between β_{4a} and $\left|\frac{1-\beta_{4a}}{\alpha_{4d}}+\frac{1-\alpha_{4d}}{\beta_{4a}}\right|$ for complete $Li_{6-a}PS_{5-a}X_{1+a}$ series.

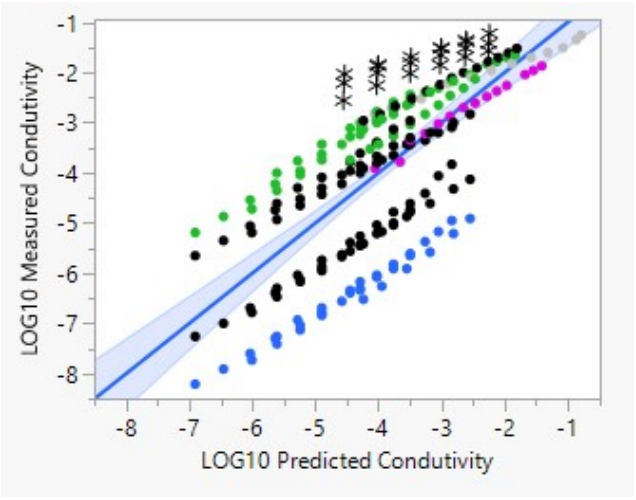

Figure S6. Measured conductivity vs multivariate predicted conductivity of the multivariate Log-Log linear regression model of $Li_{6-a}PS_{5-a}X_{1+a}$ argyrodite conductivity as function of X^- concentration and $1/T$.

2. DFT calculations

The Li^+ ion distribution within the argyrodites was studied by means of the Radial Distribution Function (RDF), g(r), of Li^+ ions with respect to the 4a and 4d sites. Figure S7 shows the RDF of Li+ for Li_6PS_5X (X=Cl) at the three considered substitution degrees. In argyrodite samples with a poor ionic potential isotropy, Li^+ ions tend to remain near 4d sites. For example, for a fully ordered Li_6PS_5X, 4a sites are not coordinated by Li^+. The peak shown by the 4a RDF at a distance of 3.62 Å, represents Li^+ ions coordinating the neighbouring 4d sites. For a disordered argyrodite (α=β=0.5 in the example above) the potential becomes more isotropic between sites and Li^+ ions become delocalized near 4d and 4a sites, but also between them.

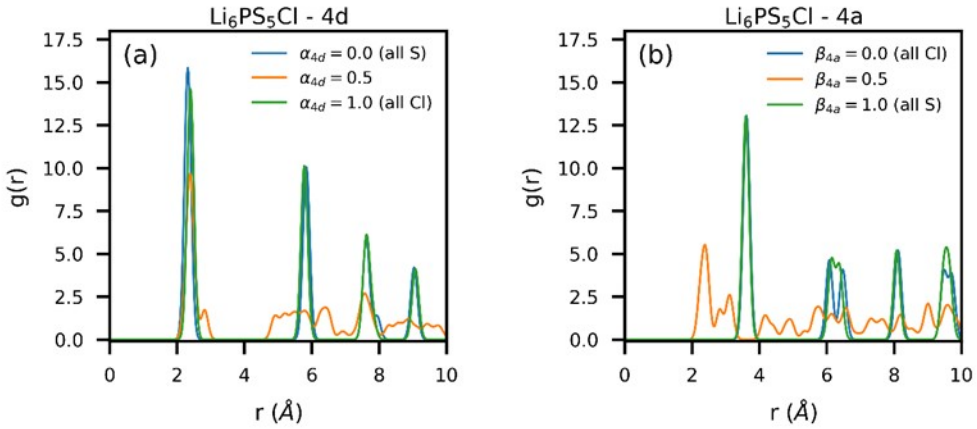

Figure S7. Radial distribution function (RDF) of Li^+ ions in Li_6PS_5Cl with respect 4d and 4a sites as a function of their X_{4d}/S_{4d} substitution level (α_{4d}, β_{4a}). (a) 4d sites. (b) 4a sites.

For disordered argyrodite samples, the potential flattens, becoming more isotropic, and spreads connecting 4a and 4d sites, as shown in Figure S8(b-d) and adjacent 4d sites, as shown in Figure S8(f-h). These regions allow Li^+ to "delocalize" and diffuse between those sites, enabling percolation between different cages and improving ionic conductivity, in accordance with our experimental results. Note that not only diffusion paths between sites occupied by different ions are activated, such as those between Cl_{4d} and S_{4a} in Figure 8(c) or between S_{4d} and Cl_{4d} in Figure 8(g), but also paths between sites occupied by similar ions, such as S_{4d} and S_{4a} in Figure 8(b) or Cl_{4d} and Cl_{4d} in Figure 8(h). The similar isotropic potential between sites occupied by similar ions further supports the enhanced conductivity of argyrodite samples in the encompassing $Li_{6-a}PS_{5-a}X_{1+a}$, for which ionic potential isotropy is not reached through disorder but rather through control of the overall chemical composition.

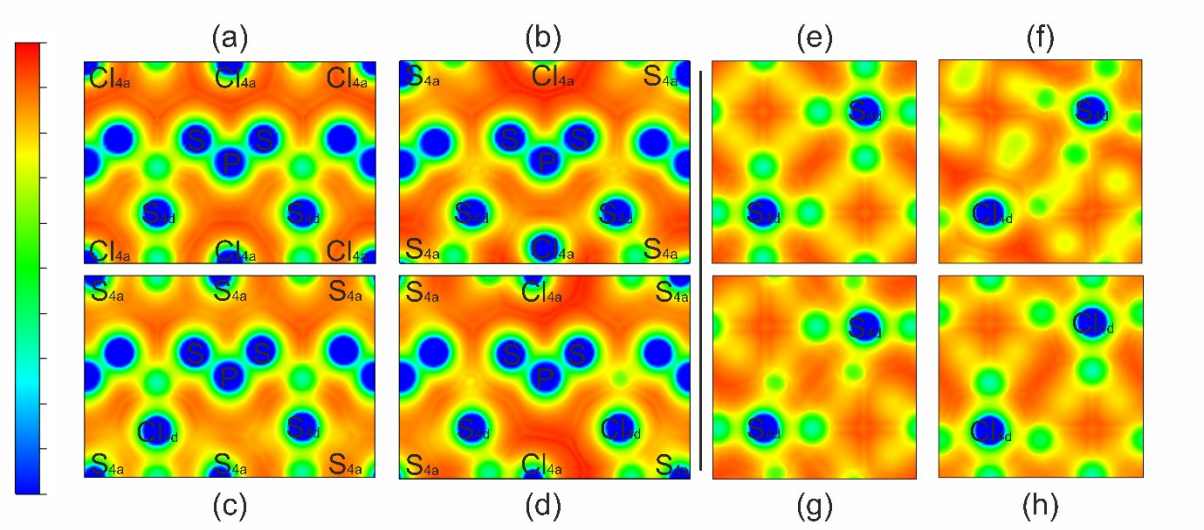

Figure S8. DFT potential between 4d-4a sites (a-d) and 4d-4d sites (e-h) in ordered ($\alpha_{4d} = \beta_{4a} = 0$) and disordered ($\alpha_{4d} = \beta_{4a} = 0.5$) Li_6PS_5Cl argyrodite. (a) 4d-4a sites in the (110) plane of an ordered Li_6PS_5X. (b-d) 4d-4a sites in different equivalent planes of a disordered Li_6PS_5X. (e) 4d-4d sites at the (001) plane at z=0.25 of an ordered Li_6PS_5X. (f-h) 4d-4d sites in different equivalent planes for a disorder of a disordered Li_6PS_5X. Li^+ cations can be identified by the cyan colour of their nuclei.